

Article

Analysis of the Catalytic Effects Induced by Alkali and Alkaline Earth Metals (AAEMs) on the Pyrolysis of Beech Wood and Corncob

Wei Wang ^{1,2} , Romain Lemaire ^{1,*}, Ammar Bensakhria ² and Denis Luart ³ ¹ Department of Mechanical Engineering, École de Technologie Supérieure, Montreal, QC H3C 1K3, Canada² Université de Technologie de Compiègne, Centre de Recherche de Royallieu, EA 4297-TIMR, BP20529, 60205 Compiègne, France³ École Supérieure de Chimie Organique et Minérale, 1 Rue du Réseau Jean-Marie Buckmaster, 60200 Compiègne, France

* Correspondence: romain.lemaire@etsmtl.ca; Tel.: +1-514-396-8727

Abstract: The catalytic pyrolysis of beech wood and corncob was experimentally investigated considering six additives containing alkali and alkaline earth metals (Na₂CO₃, NaOH, NaCl, KCl, CaCl₂ and MgCl₂). Thermogravimetric analyses (TGA) were carried out with raw feedstocks and samples impregnated with different concentrations of catalysts. In a bid to better interpret observed trends, measured data were analyzed using an integral kinetic modeling approach considering 14 different reaction models. As highlights, this work showed that cations (Na⁺, K⁺, Ca²⁺, and Mg²⁺) as well as anions (i.e., CO₃²⁻, OH⁻, and Cl⁻) influence pyrolysis in selective ways. Alkaline earth metals were proven to be more effective than alkali metals in fostering biomass decomposition, as evidenced by decreases in the characteristic pyrolysis temperatures and activation energies. Furthermore, the results obtained showed that the higher the basicity of the catalyst, the higher its efficiency as well. Increasing the quantities of calcium- and magnesium-based additives finally led to an enhancement of the decomposition process at low temperatures, although a saturation phenomenon was seen for high catalyst concentrations.

Keywords: pyrolysis; biomass; catalyst; alkali and alkaline earth metals

Citation: Wang, W.; Lemaire, R.; Bensakhria, A.; Luart, D. Analysis of the Catalytic Effects Induced by Alkali and Alkaline Earth Metals (AAEMs) on the Pyrolysis of Beech Wood and Corncob. *Catalysts* **2022**, *12*, 1505. <https://doi.org/10.3390/catal12121505>

Academic Editors: Omid Norouzi, Pietro Bartocci, Somayeh Taghavi and Shima Masoumi

Received: 14 October 2022

Accepted: 18 November 2022

Published: 24 November 2022

Publisher's Note: MDPI stays neutral with regard to jurisdictional claims in published maps and institutional affiliations.



Copyright: © 2022 by the authors. Licensee MDPI, Basel, Switzerland. This article is an open access article distributed under the terms and conditions of the Creative Commons Attribution (CC BY) license (<https://creativecommons.org/licenses/by/4.0/>).

1. Introduction

Major concerns related to global warming and greenhouse gas emissions have intensified the attention being paid to industrial applications consuming fossil fuels to produce electricity, heat, and chemicals. In this context, the use of low-emission and carbon-neutral renewable energy resources, such as biomass, has attracted interest, with a view to gradually substituting conventional fossil fuels. The net quantity of CO₂ released into the atmosphere can potentially be limited with the use of biomass, which is widely available in nature. Such CO₂ emissions occurring when using biomass tend to be balanced out by the volumes of the gas absorbed during plant growth through photosynthesis [1]. Furthermore, biomass can be converted into a wide variety of biochemicals and high-value biofuels by means of biochemical or thermochemical processes, particularly those including pyrolysis [2].

From a chemical perspective, lignocellulosic biomass is mainly composed of carbon, oxygen, and hydrogen. Other minor or trace elements, including sulfur, nitrogen, and ash, are also commonly detected in agricultural and forestry biomass. Because biomass has a much greater oxygen content than do fossil fuels (e.g., petroleum or coal), the potential use of products resulting from its raw-form thermal conversion is limited by the fact that such products often suffer from high corrosiveness, low stability, high viscosity, and a low heating value. To address these issues, an interesting option is to implement a catalytic

treatment of biomass to optimize selectivity and remove oxygenated groups in order to produce upgraded pyrolysis products [3–6]. Consequently, many catalysts, including zeolites, metal oxides, and their salts, have been considered and investigated in previous studies [3–6].

Among the above-listed catalysts, alkali and alkaline earth metals (AAEMs) are naturally present in lignocellulosic biomass. Their content depends mainly on the type of feedstock considered. Moreover, the presence of inherent or added AAEMs can significantly influence both the pyrolysis process and the composition of the so-generated products. As a consequence, many researchers have investigated the catalytic effects of AAEMs on the pyrolysis of biomass (see [7] and references therein). The method most commonly used in this context consists of the impregnation of the feedstocks into aqueous solutions of AAEM salts as this allows enhancing the interactions of the metal cations with the biomass structure through the formation of coordination bonds with the biopolymer molecules. It has notably been shown that solvated cations can penetrate biopolymers to foster depolymerization and dehydration reactions, thereby enhancing the biomass conversion. AAEM salts, including sodium chloride (NaCl), sodium carbonate (Na₂CO₃), potassium chloride (KCl), and calcium chloride (CaCl₂), moreover, exhibit a good stability under heating (as exemplified for temperatures up to 700 °C in the case of NaCl and KCl [8] and up to 800 °C for Na₂CO₃ [9]), thus making them interesting compounds for pyrolysis. During experiments focusing on the fast pyrolysis of yellow poplar impregnated with different concentrations of magnesium chloride (MgCl₂), Hwang et al. showed that divalent magnesium cations enable increasing the water content of bio-oil by dehydration, and decreasing the yield of levoglucosan, while facilitating the formation of char and oligomers [10]. Comparing the impact of four AAEM chlorides on the pyrolysis of cellulose, Shimada et al. observed that alkaline earth metals significantly lower the bulk cellulose pyrolysis temperature [8]. Alternatively, solid AAEM oxides can be added to biomass samples by dry mixing or by means of a catalytic bed. In such configurations, the volatile species released during pyrolysis can react on the surface of the catalysts, allowing oxygenated groups to be removed through deoxygenation reactions (see [6] and references therein).

Although several studies have recently been conducted to elucidate the impact of AAEMs on the pyrolysis behavior of various fuels, there is still a crucial need for direct comparisons aimed at evidencing the impact of different AAEMs added to the same feedstocks under the same operating conditions, as highlighted in a general review on the matter by [7]. It is noteworthy that while many studies investigating the catalytic effects of AAEMs have focused mainly on the chemical speciation of pyrolysis products [5–7,11], there is relatively limited research, however, that has explored the decomposition kinetics of AAEM-catalyzed feedstocks [7]. In this context, one may point to a work by Nowakowski et al., who compared the rate constant parameters derived from the TGA analysis of short rotation willow coppice (SRWC) and synthetic biomass samples [12]. Both feedstocks were pretreated to remove salts and metals using hydrochloric acid before being impregnated with potassium. In analyzing the results from the characterization of pure, acid-treated and impregnated biomass, Nowakowski et al. found that the removal of mineral matters led to an increase in the activation energies of the pyrolysis reaction, while the inverse was true with the addition of impregnated potassium, in which case it decreased. Han et al. then studied the influence of CaO additives on wheat-straw pyrolysis at three different mole ratios of carbon in wheat straw to calcium in CaO [13]. Using a first-order reaction model, the authors estimated activation energy values ranging between 70.1 and 76.6 kJ/mol for raw wheat straw and heating rates of 20 and 10 °C/min, respectively, compared to values that were ~3.6 kJ/mol lower on average for the different CaO-loaded samples. In a subsequent work, Wu et al. used six AAEM chlorides and acetates (KCl, NaCl, CH₃COOK, CH₃COONa, (CH₃COO)₂Ca·3H₂O, and (CH₃COO)₂Mg) at different concentrations to study the catalyzed pyrolysis of microcrystalline cellulose [14]. Here again, the results obtained showed that AAEMs can catalyze the pyrolysis process and hence decrease the reaction apparent activation energies, as previously observed in the

case of potassium acetate and chloride added at high concentrations [15]. Notwithstanding the consensus among the above-cited works regarding the catalytic efficiency of AAEMs, some other works have led to more mitigated conclusions. Zhou et al., for instance, recently investigated the hydrolysis behavior of pine wood samples impregnated with different potassium contents [16]. While their results demonstrated that potassium influences biomass pyrolysis, especially by modifying the maximum weight loss rates and the corresponding peak temperatures, the kinetic modeling they performed did not truly reveal any decrease in the activation energy with increasing catalyst contents.

The above brief overview of the literature illustrates the fact that, more than ever, additional studies are required in order to better understand the catalytic effects induced by AAEMs on the pyrolysis kinetics of biomass. Although we recently summarized the main mechanisms and pathways underlying the AAEM-catalyzed pyrolysis of biomass (e.g., depolymerization, dehydration, cracking, etc.) in [7], the conclusions drawn therein still highlighted the need for further research targeting a systematic assessment of the catalytic effects of different AAEM additives added to the same feedstocks under the same conditions, while ruling on the potential impact of counter anions in AAEM salts. To fill this gap, the present work presents an experimental characterization and comparison of the impacts of six AAEM compounds (NaCl, Na₂CO₃, NaOH, KCl, CaCl₂, and MgCl₂) on the decomposition behavior of beech wood and corncob. To this end, thermogravimetric analyses (TGA) were carried out with pure feedstocks as well as with biomass samples impregnated with the above-listed catalysts at different loads. In addition to examining the effect of the considered AAEMs on the characteristic pyrolysis temperatures and mass loss rates, this paper also includes an analysis aimed at investigating the relative impact of alkali and alkaline earth metals on pyrolysis kinetics. Finally, the influence of the catalyst content is investigated in a bid to rule on the existence of saturation phenomena. This experimental study will therefore provide a general picture of the relative effects associated with the impregnation of two biomass resources with six different AAEM catalysts, while interpreting observed trends, notably through a global kinetic modeling approach. As such, this study will contribute to addressing one of the bottlenecks hindering our assessment of the impact of AAEMs, as identified in [7], where diverging trends were sometimes reported from one study to another due to the evaluation of data derived from the implementation of widely varied feedstocks and operating conditions.

2. Materials and Methods

2.1. Feedstocks

The proximate and ultimate analyses of the beech wood and corncob samples studied herein are provided in Table 1. Samples were prepared as detailed in [17,18]. Specifically, corncob (without corn grain) and beech wood (without bark) were ground and sieved into a size fraction of 40–125 µm. These feedstocks, obtained from the French forestry and agriculture industries, respectively, are known to contain inherent inorganic elements including Na, K, Ca, and Mg, whose contents have been estimated to be of the order of 100, 3600, 2000, and 600 ppm (dry basis) in beech wood [19], versus 300, 6300, 300, and 400 ppm in corncob [20]. As far as the biochemical composition of these biomass resources is concerned, the data reported in [21,22] show that the mass fractions of cellulose, hemicellulose, lignin and extractives in beech wood typically reach mean values of ~43.6%, ~29.1%, ~23.7, and ~3.1%, respectively, as compared to values of ~34.2%, ~40.8%, 14.3%, and ~7.6% for corncob based on the results obtained from [21,23,24].

Table 1. Proximate and ultimate analyses of beech wood and corncob samples.

Sample	Proximate Analysis			Ultimate Analysis					
	Fixed Carbon (wt%, db [†])	Volatiles (wt%, db)	Ash (wt%, db)	C (wt%, daf [‡])	H (wt%, daf)	O * (wt%, daf)	N (wt%, daf)	S (wt%, daf)	Cl (wt%, daf)
Beech wood	14.36	84.48	1.16	51.6	5.4	43.0	-	-	-
Corncob	13.47	85.05	1.48	47.5	6.0	42.9	0.6	0.42	2.58

[†] db: dry basis; [‡] daf: dry ash-free basis; * calculated by difference.

Six AAEM compounds (NaCl, Na₂CO₃, NaOH, KCl, CaCl₂, and MgCl₂) were selected as catalysts. This allowed to study and compare the catalytic influence of both the cations (Na⁺, K⁺, Mg²⁺, or Ca²⁺) and anions (Cl⁻, CO₃²⁻, or OH⁻) on the pyrolysis kinetics. To foster interactions between the cations and biomass, the samples were prepared by wet impregnation, as was done in [16,25–30]. In a first step, experiments aimed at comparing the effects induced by each catalyst were performed by impregnating the samples with exactly the same amounts of metal ions for each AAEM compound. To this end, the different metal chlorides were mixed with distilled water to obtain solutions having initial metal atom concentrations (noted Y₀) of 0.22 mol/L for NaCl, Na₂CO₃, NaOH, 0.13 mol/L for KCl and CaCl₂, versus 0.21 mol/L for MgCl₂, respectively, (i.e., 5 g of metal ions per liter of solution). By impregnating 4 g of biomass in 40 mL of solution as an example (i.e., 10 mL/g, as in [30]), a ratio between the mass of cations and the mass of biomass of 0.05 (i.e., 1:20 as implemented in [28]) was obtained. In a second step, the amounts of catalyst used for the AAEM compounds identified as being the most effective at enhancing the biomass degradation were varied to allow investigating their catalytic effect, depending on their relative content. To that end, solutions having metal concentrations of 0.1 × Y₀, 0.5 × Y₀, and 2 × Y₀ were used. Since impregnation allows metal ions to be in contact with the biopolymers and to bind to active sites through ion-exchange mechanisms [31,32], varying the concentration of the catalysts in the impregnation solutions as in [30,33] thus allowed investigating the relative impact of such content on the promotion of the interactions between the biomass and the metal ions. Regarding the impregnation process, tested feedstocks were mixed within the catalyst solutions and stirred for two hours, as in [16], using a magnetic stirrer. For control samples (i.e., raw beech wood and corncob samples), they were suspended in deionized water for the same duration and within the same stirring conditions to exclude the influence of water washing. Impregnated samples were finally filtered to eliminate the extra cations and anions remaining in the solution before being dried in an oven at 105 °C, as recommended in [26,28–30], for 24 h.

2.2. Thermogravimetric Analyses (TGA)

Non-isothermal pyrolysis experiments were carried out using a SETARAM SETSYS Evolution TGA thermogravimetric analyzer. Following [16], among others, samples weighing around 10 mg were placed in alumina crucibles before being thermally treated at a constant heating rate (β) of 10 °C/min. A 100 mL/min flow of helium was used to continuously maintain an inert environment during the experiments. The samples were heated from 20 °C up to 105 °C for 20 min to ensure the complete removal of free water. The temperature was then continuously increased up to 700 °C. As for the conversion degree (α) at any given time (t), it was calculated as in [13,16,29,34] from the initial (i) and final (f) residual masses (noted TG and expressed in wt%) based on Equation (1):

$$\alpha = \frac{TG_i - TG_t}{TG_i - TG_f} \quad (1)$$

where the measurement point, corresponding to a temperature of 106 °C, was defined as the initial time (i) and related to a 0% conversion degree, while the final point (f), corresponding to a temperature of 700 °C, was associated with a 100% conversion degree. Eventually, and

based on uncertainties assessed in [17,18], a mean relative deviation of the order of $\pm 1.34\%$ was estimated on measured weight losses considering a 95% confidence level.

2.3. Kinetic Modeling of TGA Results

The theoretical evolution of the conversion degree as a function of the temperature (T) follows an Arrhenius-like equation of the type:

$$\frac{d\alpha}{dT} = \frac{A}{\beta} \times \exp\left(-\frac{E_a}{R \times T}\right) \times f_{(\alpha)} \quad (2)$$

where A stands for the frequency factor of the rate constant, E_a denotes the activation energy, R corresponds to the universal gas constant, while $f_{(\alpha)}$ is the differential reaction model (see Table 2).

Table 2. Summary of some commonly used reaction models [35,36].

Class of Reaction Model	Denomination	Differential Form $f_{(\alpha)}$	Integral Form $g_{(\alpha)}$
Order-based	Mampel first-order (F1) [†]	$(1 - \alpha)^1$	$-\ln(1 - \alpha)$
	nth-order (Fn) [†]	$(1 - \alpha)^n$	$[1 - (1 - \alpha)^{1-n}]/(1 - n)$
Diffusion	1-D diffusion (D1) [†]	$1/2 \times \alpha^{-1}$	α^2
	2-D diffusion (D2) [†]	$[-\ln(1 - \alpha)]^{-1}$	$(1 - \alpha) \times \ln(1 - \alpha) + \alpha$
	3-D diffusion Jander (D3) [†]	$3/2 \times (1 - \alpha)^{2/3} \times [1 - (1 - \alpha)^{1/3}]^{-1}$	$[1 - (1 - \alpha)^{1/3}]^2$
	3-D diffusion Ginstling-Brounshtein (D4)	$3/2 \times [(1 - \alpha)^{-1/3} - 1]^{-1}$	$1 - 2/3 \times \alpha - (1 - \alpha)^{2/3}$
Geometrical contraction	Contracting cylinder (R2) [†]	$2 \times (1 - \alpha)^{1/2}$	$1 - (1 - \alpha)^{1/2}$
	Contracting sphere (R3) [†]	$3 \times (1 - \alpha)^{2/3}$	$1 - (1 - \alpha)^{1/3}$
Nucleation	Avrami-Erofeev (A2) [†]	$2 \times (1 - \alpha) \times [-\ln(1 - \alpha)]^{1/2}$	$[-\ln(1 - \alpha)]^{1/2}$
	Avrami-Erofeev (A3) [†]	$3 \times (1 - \alpha) \times [-\ln(1 - \alpha)]^{2/3}$	$[-\ln(1 - \alpha)]^{1/3}$
	Avrami-Erofeev (A4) [†]	$4 \times (1 - \alpha) \times [-\ln(1 - \alpha)]^{3/4}$	$[-\ln(1 - \alpha)]^{1/4}$
Power law	2-Power law (P2) [†]	$2 \times \alpha^{1/2}$	$\alpha^{1/2}$
	3-Power law (P3)	$3 \times \alpha^{2/3}$	$\alpha^{1/3}$
	4-Power law (P4)	$4 \times \alpha^{3/4}$	$\alpha^{1/4}$

[†] Models tested in the present work.

Actually, the modeling of TGA results obtained as part of this analysis are intended to aid the interpretation of measured data through the assessment of the relative impact of the tested catalysts on the kinetic parameters governing the overall pyrolysis process, including the activation energy. The latter indeed reflects the minimum energy required for a reaction to occur. As a consequence, the more the E_a decreases as a result of the addition of AAEM compounds, the less the external energy required to overcome the energy barrier allowing the pyrolysis to take place, and the greater the catalytic effect. In order to evidence such a phenomenon from a kinetic point of view, the Coats–Redfern integral method was selected. This approach, which is widely implemented to simulate biomass pyrolysis [13,16,28,37–46], has proven to be useful for inferring activation energy and frequency factor values from non-isothermal analyses. As such, this model-fitting method appears to be well suited to meet the objectives of the present work, which does not claim to estimate kinetic parameters intended to be valid on extended ranges of operating conditions since such an estimation would require conducting additional measurements with different β values, as we did in [47], for instance. Besides, we recently conducted a preliminary analysis based on the implementation of the Ozawa–Flynn–Wall (OFW) and Kissinger–Akahira–Sunose (KAS) isoconversional methods to analyze TGA results obtained from pyrolysis tests performed with raw beech wood and samples impregnated with NaCl, KCl and MgCl₂ [18]. Results reported therein especially showed inferred activation energies varying within a narrow range for conversion degrees up to ~80%, thus strengthening the relevance of the one-step global kinetic approach adopted herein for comparison purposes, as mentioned above.

The theoretical background underlying the implementation of the Coats–Redfern method [48] can be summarized as follows. First, one can obtain the expression of the integral form of the reaction model $g(\alpha)$ depicted in Equation (3) by integrating both sides of Equation (2) while assuming an order-based reaction model of the form $(1 - \alpha)^n$, in addition to setting the initial temperature and conversion degree to zero.

$$g(\alpha) = \int_0^\alpha \frac{d\alpha}{f(\alpha)} = \int_0^\alpha \frac{d\alpha}{(1 - \alpha)^n} = \frac{A}{\beta} \times \int_{T_0}^T \exp\left(-\frac{E_a}{R \times T}\right) dT \cong \frac{A}{\beta} \times \int_0^T \exp\left(-\frac{E_a}{R \times T}\right) dT \quad (3)$$

Using an algebraic approximation of the right-hand side integral term of Equation (3), the following expression is then obtained:

$$\frac{1 - (1 - \alpha)^{1-n}}{1 - n} = \frac{A \times R \times T^2}{\beta \times E_a} \left[1 - \frac{2 \times R \times T}{E_a} \right] \times \exp\left(-\frac{E_a}{R \times T}\right) \quad (4)$$

hence leading to Equations (5) and (6) for $n \neq 1$ and $n = 1$, respectively:

$$\ln \left[\frac{1 - (1 - \alpha)^{1-n}}{T^2 \times (1 - n)} \right] = \ln \left[\frac{A \times R}{\beta \times E_a} \left(1 - \frac{2 \times R \times T}{E_a} \right) \right] - \left(\frac{E_a}{R \times T} \right) \quad (5)$$

$$\ln \left[-\frac{\ln(1 - \alpha)}{T^2} \right] = \ln \left[\frac{A \times R}{\beta \times E_a} \left(1 - \frac{2 \times R \times T}{E_a} \right) \right] - \left(\frac{E_a}{R \times T} \right) \quad (6)$$

Based on the above integral form, Equation (3) can be converted as a linear regression that plots $\ln \left[\frac{g(\alpha)}{T^2} \right]$ as a function of $\frac{1}{T}$:

$$\ln \left[\frac{g(\alpha)}{T^2} \right] = \ln \left[\frac{A \times R}{\beta \times E_a} \left(1 - \frac{2 \times R \times T}{E_a} \right) \right] - \frac{E_a}{R \times T} \quad (7)$$

Since the term $\frac{2 \times R \times T}{E_a}$ can be assumed to be equal to zero, Equation (7) can finally be simplified as follows:

$$\ln \left[\frac{g(\alpha)}{T^2} \right] = \ln \left[\frac{A \times R}{\beta \times E_a} \right] - \frac{E_a}{R \times T} \quad (8)$$

If the selected reaction model is adapted to account for the investigated decomposition process, plotting the left-hand term of Equation (8) as a function of $1/T$ should lead to obtaining a straight line whose slope corresponds to the value of $-E_a/R$, hence allowing to estimate the apparent activation energy E_a . Finally, the value of the pre-exponential factor A can be inferred simply based on the intercept (i.e., $\ln[A \times R/(\beta \times E_a)]$).

3. Results and Discussion

3.1. TGA Results

The evolutions of the mass loss (TG) and the mass loss rate (dTG) of both treated and untreated beech wood samples are depicted in Figure 1 as a function of the temperature. Results from the analysis of the raw feedstock (corresponding to the control sample) are first compared therein with those obtained for samples impregnated with sodium additives (i.e., NaCl, Na₂CO₃ and NaOH) added using solutions at Y_0 mol of Na⁺ per liter (see Section 2.1). In addition, Table 3 also brings together the values of the maximum mass loss rate (dTG_{max}) and characteristic pyrolysis temperatures, which include the temperature for which a dTG peak is recorded (T_p), as well as the initial and final temperatures (noted T_i and T_f), representing the temperatures measured for conversion degrees of 10 and 80%, respectively.

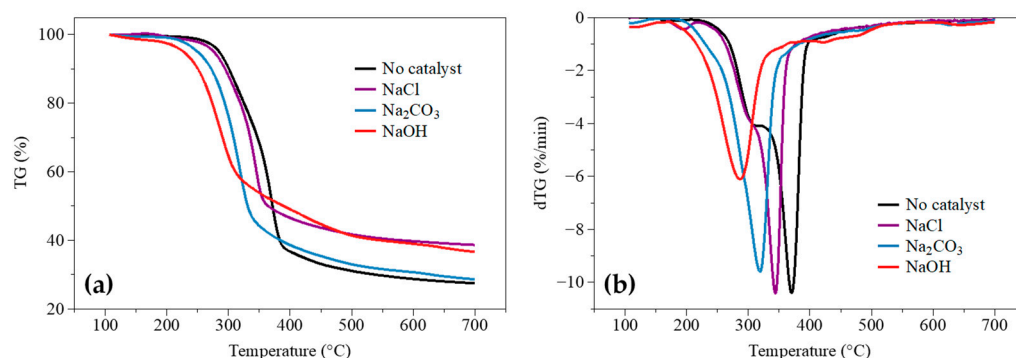


Figure 1. Evolution of (a) the mass loss (TG) and (b) the mass loss rate (dTG) as a function of the temperature for raw beech wood (noted “No catalyst”) and samples impregnated with NaCl, Na₂CO₃, and NaOH solutions at Y₀.

Table 3. Maximum mass loss rate (dTG_{max}) and characteristic temperatures determined by TGA for raw beech wood and samples impregnated with NaCl, Na₂CO₃ and NaOH solutions at Y₀.

Sample	dTG _{max} (wt%/min)	T _i (°C)	T _f (°C)	T _p (°C)
Beech wood	−4.09 [†] ; −10.37	293	380	322 [†] ; 371
Beech wood + NaCl	−4.05 [†] ; −10.38	281	359	307 [†] ; 344
Beech wood + Na ₂ CO ₃	−9.60	261	359	319
Beech wood + NaOH	−6.11	235	398	287

[†] shoulder values.

Looking at the results reported in Figure 1 and Table 3, it can first be noted that the conversion of raw beech wood starts at around 293 °C. The mass loss then rapidly increases before plateauing above 380 °C. The peak of the dTG curve is observed at 371 °C, with a shoulder located on the left for a temperature of 322 °C (see Figure 1b and Table 3). Such overlapping peaks actually produce a single dTG peak with a lower temperature shoulder, which represents the decomposition of hemicellulose, and a higher temperature peak which accounts for the decomposition of cellulose [49], followed by a tailing above 400 °C that corresponds to the slow decomposition of lignin. This latter occurs over a broad range of temperatures, thus providing a gently sloping baseline to the dTG curve [50]. Significant changes in terms of curve shape and characteristic temperatures are observed for the impregnated samples. The three sodium additives notably shift the pyrolysis reactions to lower temperatures (as can be seen in Figure 1, and as exemplified by the lower T_p values reported in Table 3). Interestingly enough, the ability of the considered catalysts to decrease T_i and T_p follows their respective basicity (i.e., NaOH > Na₂CO₃ > NaCl). The use of NaOH thus induces the most significant decrease of T_p, whose value goes from 371 °C for the control sample to 287 °C for the impregnated one, thus illustrating the strong capacity of NaOH to promote low-temperature biomass conversion. It is also noteworthy that both NaOH and Na₂CO₃ allow suppressing the shoulder on the left of the main dTG peak. Alternatively, the addition of NaCl only slightly reduces the reaction temperatures and does not significantly impact the form of the TG and dTG curves, as well as the value of the mass loss rates, as compared to the control sample. Finally, it can be added that the impregnation of beech wood with the different sodium catalysts has only a limited impact on the final pyrolysis temperatures (T_f), as shown in Table 3.

Regarding the analysis and interpretation of the obtained trends, it is firstly noteworthy that the dependence of the characteristic temperatures on the catalyst basicity is consistent with observations drawn in previous studies. For instance, Wang et al. pretreated different types of lignocellulosic biomass (namely, pine wood, cotton stalk, and fir wood) with NaCl, Na₂CO₃, and NaOH [25]. The authors then reported that the peak temperature measured in the case of cotton stalk (~340 °C) tends to decrease to values of ~330, ~290, and ~280 °C when impregnating the raw biomass with NaCl, Na₂CO₃, and NaOH, respectively. As is

the case in the present work, the observed temperature reduction was shown to follow the compounds' basicity sequence (i.e., $\text{NaOH} > \text{Na}_2\text{CO}_3 > \text{NaCl}$). Actually, the effect induced by Na-containing catalysts can be related to the role of sodium ions, which are able to penetrate into the biomass textures and foster dehydration, depolymerization, ring scission, as well as rearrangement reactions of the biopolymers [25,51]. As a result, thermal decomposition occurs at lower temperatures, as observed herein as well as in [25,26,51]. Basic sodium-containing catalysts, moreover, tend to promote yields of low molecular species, as is the case with NaOH, which is likely to react through active alcohol groups of cellulose [25]. Peng et al. also explained in [52] that alkaline catalysts (such as NaOH and Na_2CO_3) are likely to promote decarboxylation or decarbonylation reactions together with the removal of unsaturated alkyl branch chains. Furthermore, NaOH, which exhibits the strongest basicity, was shown in [52] to foster the deoxygenation of methoxy groups, thus leading to phenols free of methoxy groups in the so-derived pyrolysis products. It may further be noted that such an impact of the catalyst basicity on pyrolysis enhancement was also illustrated in [52–54], where basic catalysts were proven to have a strong deoxygenation capability through decarboxylation, decarbonylation, and demethoxylation reactions. All these observations thus contribute to explaining and supporting the consistency of the trends depicted in Figure 1 and Table 3.

Nevertheless, the results reported in Figure 1 also illustrate that NaOH and NaCl tend to decrease the yield of volatile products. Data depicted in Figure 1b, moreover, illustrate the existence of a selective role of the anions in the acceleration of the decomposition of extractives, hemicellulose, and cellulose, as evidenced by the temperature for which the dTG peak is recorded, which is lower for NaOH than for Na_2CO_3 and NaCl. NaOH is notably evidenced to induce a selective promotion of the decomposition of extractives and hemicellulose which typically takes place below 250 °C and 350 °C, respectively, [55–57] in agreement with the trend shown in Figure 1. This observation is consistent with the fact that NaOH has proven to favor the extraction of some low molecular compounds at low temperatures due to its high basicity [25]. Furthermore, NaOH is also prone to solubilize lignin and hemicellulose by breaking the ester bonds of the lignin-carbohydrate complex in addition to inducing swelling of lignocellulose, while for its part, cellulose (which decomposes between 260 and 400 °C) tends to remain relatively unaffected [58]. Alternatively, Na_2CO_3 and NaCl are more likely to have a catalytic effect on the dehydration and bond scissions taking place inside and outside the rings in the cellulose chain, thus resulting in an increased rate of degradation of this biopolymer [59]. For the residual mass measured with NaCl, which is higher than that measured with raw beech wood, this observation could be related to the fact that sodium chloride can reduce the levoglucosan (LG) yields from cellulose induced by the polymerization of volatile LG, which in turn enhances the char formation as reported in [60,61].

To complement the results obtained with sodium additives as a first step, additional analyses were carried out with a series of beech wood and corncob samples impregnated with NaCl, KCl, CaCl_2 , and MgCl_2 . Proceeding as such allowed to directly compare the catalytic effect related to the four cations contained in these AAEM catalysts (i.e., Na^+ , K^+ , Ca^{2+} , and Mg^{2+}). As far as beech wood samples are concerned, the initial and peak pyrolysis temperatures are shown to decrease with all the catalysts, as compared to the test performed with the untreated wood sample (see Figure 2 and Table 4). This result is actually in line with the catalytic effects induced by AAEMs, which are known to decrease the reaction temperatures, enhance the biopolymer decomposition, and foster the formation of gaseous species, even at low additive loading ratios [8,10,14,27,30,60,62–64].

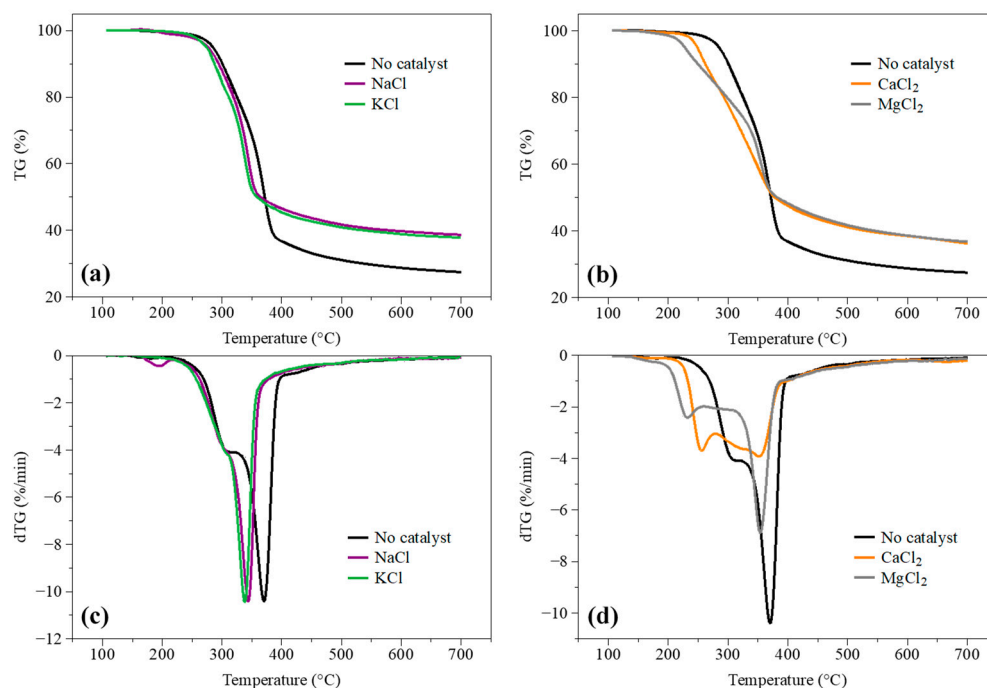


Figure 2. Evolution of (a,b) the mass loss (TG) and (c,d) the mass loss rate (dTG) as a function of the temperature for raw beech wood (noted “No catalyst”) and samples impregnated with NaCl and KCl (a,c) as well as CaCl₂ and MgCl₂ (b,d) solutions at Y₀.

Table 4. Maximum mass loss rate (dTG_{max}) and characteristic temperatures determined by TGA for raw beech wood and samples impregnated with NaCl, KCl, CaCl₂, and MgCl₂ solutions at Y₀.

Sample	dTG _{max} (wt%/min)	T _i (°C)	T _f (°C)	T _p (°C)
Beech wood	−4.09 [†] ; −10.37	293	380	322 [†] ; 371
Beech wood + NaCl	−4.04 [†] ; −10.38	281	359	307 [†] ; 344
Beech wood + KCl	−4.13 [†] ; −10.45	278	356	306 [†] ; 338
Beech wood + CaCl ₂	−3.67 [†] ; −3.88	252	385	258 [†] ; 355
Beech wood + MgCl ₂	−2.40 [†] ; −6.83	233	388	234 [†] ; 355

[†] Values related to the shoulder and/or to the first dTG peak.

More specifically, metallic ions have the potential to be adsorbed into biopolymers and interact with oxygenated functional groups to induce homolytic fission of glucose rings, cleavage of glycosidic bonds, and dehydration reactions [27,60,62,65]. Relatively significant differences can be observed, however, between the behavior of alkali and alkaline earth metals. Compared to alkali metals, alkaline earth metals indeed shift the pyrolysis process to lower temperatures. This is exemplified by the T_i value (see Table 4), which goes from 293 °C for the raw biomass to 252 °C and 233 °C for the samples impregnated with CaCl₂ and MgCl₂, respectively (thus representing decreases of ~14 and ~20%), versus 281 °C and 278 °C for the samples treated with NaCl and KCl (hence corresponding to reductions of only ~4 and ~5%). Similarly, the T_p value (when considering the shoulder) falls from ~20 to ~27% for samples impregnated with CaCl₂ and MgCl₂, versus ~5% with NaCl and KCl. In addition, alkaline earth metals also induce significant changes in the shape of the weight loss and weight loss rate curves (see Figure 2). The shoulder observed on the left of the main dTG peak indeed tends to disappear for CaCl₂- and MgCl₂-impregnated samples in favor of the formation of two separate peaks concomitantly to the widening of the dTG curves for temperatures between 200 and 400 °C. Inversely, relatively few changes can be seen when looking at the curves obtained with the samples impregnated with alkali metals. Results depicted in Figure 2, moreover, show that alkaline earth metals tend to affect the decomposition of hemicellulose in a selective way, while alkali metals more

significantly influence that of cellulose. Actually, this observation is consistent with the fact that divalent cations, such as those contained in MgCl_2 , are prone to enhance the degradation of hemicellulose [66] while promoting repolymerization reactions, leading to increased char formation (as suggested when comparing the TG curves obtained with raw and impregnated samples) [10]. In fact, magnesium was especially demonstrated in [10] to influence the decomposition of hemicellulose as well as the initial decomposition of cellulose. According to Hwang et al., magnesium in biomass could combine with the oxygen-containing functional groups and linkages at surface molecules, thus facilitating the decomposition of biomass constituents at low temperatures (as observed herein) through the weakening of the intramolecular bond strength. As for KCl and NaCl, they have proven to be more prone than CaCl_2 and MgCl_2 to decompose LG, which is a typical cellulose pyrolysis product [60]. The mechanism underlying this phenomenon is likely related to the modification of the cellulose structure in biomass impregnated with alkali metals, which increases its reactivity while decreasing the thermal decomposition temperature, thus, here again, corroborating the above observations [30]. The fact that alkaline earth metals generally show a better catalytic effect on the pyrolysis of biomass as compared to alkali metals may be related to the strong affinity of the former to oxygenated groups present in the biopolymers and to the ability of metal ions to foster the deoxygenation process of biomass via dehydration, together with the depolymerization of hemicellulose and cellulose [27,64,66,67]. This therefore explains the stronger ability of alkaline earth metals to reduce the characteristic pyrolysis temperatures, as observed in the present work as well as in [8,27,66]. Shimada et al. especially observed such a trend when analyzing the influence of different AAEMs (NaCl, KCl, CaCl_2 , and MgCl_2) on the pyrolysis of cellulose [8]. Comparing the effects of three metal chlorides (NaCl, ZnCl_2 , and MgCl_2) on the pyrolysis of soybean hulls, Santana et al. similarly concluded that the addition of MgCl_2 led to more significant decreases in the decomposition temperature as compared to NaCl [66].

Regarding the analyses conducted with corncob, the results reported in Figure 3 and Table 5 show that the decomposition of this feedstock occurs at temperatures lower than those encountered in the case of beech wood. The conversion of the raw corncob sample indeed takes place at temperatures between 268 and 357 °C (i.e., ~24 °C lower on average than those measured with beech wood (see Tables 4 and 5)). This lower range of temperatures may be related to the higher ash content of agricultural crops, which may promote the thermal degradation process [68,69]. This explanation is, however, not sufficient herein, considering the minor difference in ash content between the two tested feedstocks (1.48 wt% for corncob as compared to 1.16 wt% for beech wood, as reported in Table 1). On the other hand, it is well known that agricultural crops typically contain less cellulose than hardwood, and much more extractives [69], as confirmed in Section 2.1. This difference in chemical composition could hence justify the trends described above as the thermal decomposition of cellulose essentially occurs for temperatures between 260 and 400 °C, while that of extractive is mainly active below 250 °C as mentioned above [55–57]. This interpretation is corroborated by the fact that the maximum mass loss rate measured with beech wood (−10.37 wt%/min) is ~71% higher than that for corncob (−6.07 wt%/min), thus implying that the woody biomass is richer in biopolymers that decompose at higher temperatures (T_p being indeed 371 °C for the woody biomass, versus 321 °C for the agricultural crop (see Tables 4 and 5)). It could be added that the shoulder dTG peak is measured at a lower temperature in the case of corncob (282 °C instead of 322 °C), while being related to a higher mass loss rate (−4.22 versus −4.09 wt%/min), which, here again, is consistent with the above statement regarding the higher proportion of extractives and hemicellulose in corncob.

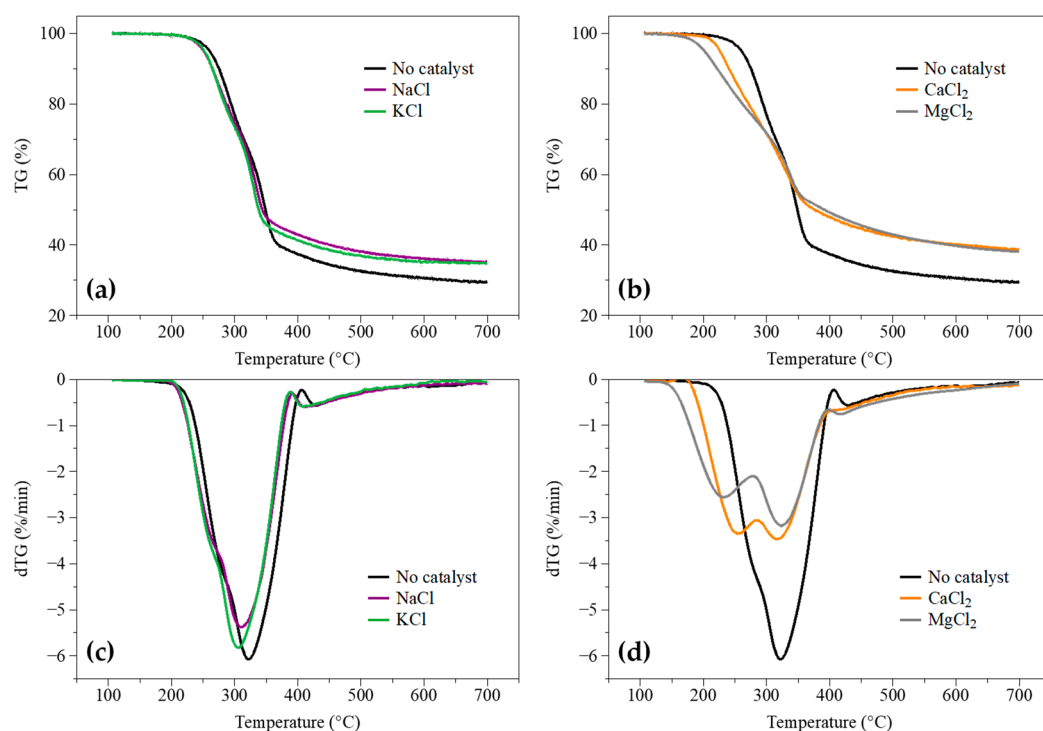


Figure 3. Evolution of (a,b) the mass loss (TG) and (c,d) the mass loss rate (dTG) as a function of the temperature for raw corncob (noted “No catalyst”) and samples impregnated with NaCl and KCl (a,c) as well as CaCl₂ and MgCl₂ (b,d) solutions at Y₀.

Table 5. Maximum mass loss rate (dTG_{max}) and characteristic temperatures determined by TGA for raw corncob and samples impregnated with NaCl, KCl, CaCl₂, and MgCl₂ solutions at Y₀.

Sample	dTG _{max} (wt%/min)	T _i (°C)	T _f (°C)	T _p (°C)
Corncob	−4.22 [†] , −6.07	268	357	282 [†] , 321
Corncob + NaCl	−3.79 [†] , −5.38	256	349	275 [†] , 311
Corncob + KCl	−3.93 [†] , −5.83	257	342	271 [†] , 305
Corncob + CaCl ₂	−3.35 [†] , −3.46	230	367	256 [†] , 318
Corncob + MgCl ₂	−2.55 [†] , −3.15	207	386	234 [†] , 327

[†] Values related to the shoulder and/or to the first dTG peak.

As for the results obtained from the analysis of impregnated corncob samples, the conclusions previously drawn in the case of beech wood still apply. Indeed, T_i and T_p tend to decrease when adding AAEM catalysts, as illustrated in Figure 3 and Table 5. This trend is particularly striking in the case of CaCl₂ and MgCl₂, as was the case for woody biomass. The shoulders in the dTG curves are indeed shifted to lower temperatures, while distinct peaks appear at 256 and 234 °C for CaCl₂ and MgCl₂, respectively, due to an enhanced decomposition of hemicellulose, which typically occurs between 190 °C and 350 °C [55,56]. As a result, while a sharp peak was observed in the case of the control sample, the width of the dTG curves increased significantly between 200 and 400 °C for CaCl₂- and MgCl₂-impregnated corncob samples. Finally, and as exemplified in Figure 3a,c, alkali metals still show limited effects on low-temperature pyrolysis as compared to alkaline earth metals.

3.2. Impact of AAEMs on Pyrolysis Kinetics

3.2.1. Catalytic Effects of AAEMs on Pyrolysis Kinetic Parameters

Following the methodology described in Section 2.3, 14 reaction models, namely, F1, F2, F3, F5, F7, D1, D2, D3, R2, R3, A2, A3, A4, and P2 (see Table 2), were selected to derive the kinetic parameters related to the pyrolysis of untreated and treated biomass samples.

To this end, curves depicting the evolution of $\ln\left[\frac{g(\alpha)}{T^2}\right]$ as a function of $\frac{1}{T}$ were plotted for each model. The slope and intercept of the straight lines obtained then led to the estimation of the activation energy (E_a) and frequency factor (A) values, respectively, as explained in Section 2.3. For brevity, only a few examples of E_a and A values inferred for the different reaction models are summarized in Table A1 provided in the Appendix A.

The obtained results first show that although the activation energies and frequency factors reported in Table A1 cover a large range of values, the efficiency of the tested catalysts (represented by their ability to shift the pyrolysis reactions to lower temperatures) follows the same sequence (with $E_a(\text{MgCl}_2) < E_a(\text{CaCl}_2) < E_a(\text{NaOH}) < E_a(\text{control sample})$), regardless of the reaction model considered. While being in line with the trends reported in Section 3.1, this observation also demonstrates that the modeling approach considered herein is well suited to meet the objectives of the present study as it allows accounting for the relative impact of tested catalysts on the pyrolysis process, regardless of the $g(\alpha)$ expression. Furthermore, and based on the obtained coefficients of determination (R^2) (see Table A1), the D3 reaction model can be identified as the most suited to fit experimentally monitored data for both beech wood and corncob. This is consistent with the fact that diffusion-based models have often been identified as being appropriate to simulate the pyrolysis of biomass [18,40,70,71].

Looking in detail at the E_a values obtained with the D3 model for raw samples, it is noteworthy that the activation energy found in the case of beech wood is higher than that estimated for corncob (i.e., 150.1 kJ/mol against 132.5 kJ/mol). As discussed in Section 3.1, this may be related to the chemical composition of these feedstocks, which is significantly different in each case (the woody biomass being richer in cellulose whose breakage requires more energy, higher temperatures and thus, a higher activation energy). Furthermore, a drop in the activation energy (−34.3 kJ/mol) can be noted when adding NaOH (see Table A1), which is in line with the above comments regarding the influence of this basic catalyst on the shift of the pyrolysis to lower temperatures. As for the catalytic effect related to the AAEM cations, the obtained results predict a catalytic efficiency following the order: $\text{Mg}^{2+} > \text{Ca}^{2+} > \text{Na}^+ > \text{K}^+$, in agreement with the observations made in Section 3.1 (see data related to corncob in Table A1). The strong ability of CaCl_2 and MgCl_2 to shift the pyrolysis to lower temperatures is, moreover, exemplified by the E_a values, which go from 150.1 to 89.4 and 75.2 kJ/mol, respectively, in the case of beech wood, versus 132.5 to 77.9 and 59.1 kJ/mol in the case of corncob (see Table A1).

To complement this preliminary analysis based on raw rate constant parameters, in Figure 4, we have also plotted the evolution of the rate constant ($k = A \times \exp(-E_a/(R \times T))$) of each sample as a function of the temperature. The obtained results confirm that CaCl_2 , MgCl_2 , and NaOH significantly increase k at low temperatures. This is actually consistent with the lower T_i and T_p values reported in Section 3.1 during the tests performed with these catalysts. The observed enhancement of k , however, vanishes at higher temperatures, which here again, is in line with the higher T_f values measured with samples impregnated with CaCl_2 and MgCl_2 , for instance. As for monovalent Na^+ and K^+ cations, Figure 4b shows that their impact is much weaker at low temperatures. While corroborating the observations in Section 3.1, this trend indicates that contrary to alkaline earth metals, which greatly influence the pyrolysis process, the catalytic effect of alkali metals is less significant (especially at low temperatures), in agreement with the fact that divalent cations have a higher affinity to oxygenated structures [10,72]. Consequently, alkaline earth metals can more easily break the inter- and intramolecular links of the biopolymers to promote reactions occurring at low temperatures [66]. On the other hand, and although being quite limited below 330 °C (see Figure 4a,b), the impact of Na_2CO_3 , NaCl, and KCl becomes more significant than that of CaCl_2 or MgCl_2 for higher heating conditions. This may notably explain why the T_f values related to such alkali metals are lower than those measured with calcium and magnesium chlorides, whose effect is weaker over this specific temperature range.

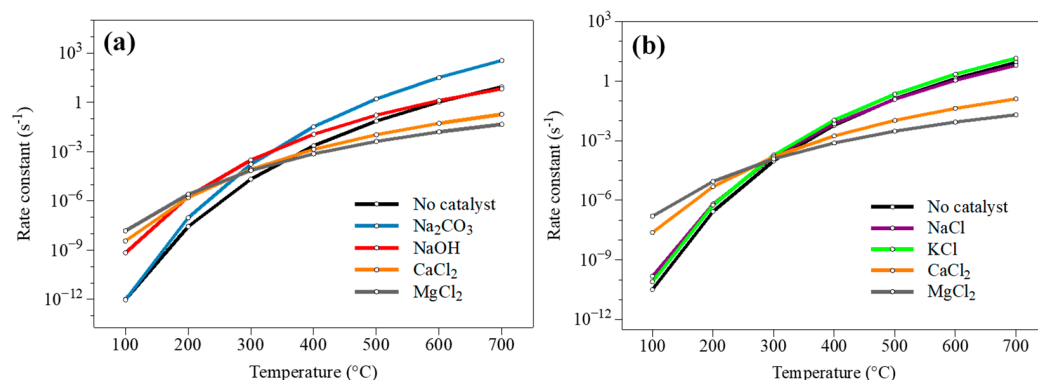


Figure 4. Variation of the rate constant k as a function of the temperature for (a) beech wood and (b) corncob samples.

Despite the somewhat limited number of kinetic studies focusing on the comparison of the catalytic effects induced by AAEMs on biomass pyrolysis [7], there is a consensus regarding the ability of alkaline earth metals to decrease E_a [13,14,18,28]. Contradictory trends have, however, been reported regarding the impact of alkali metals. For instance, Nowakowski et al. noted significant decreases of E_a (up to 50 kJ/mol) when adding KCl to short rotation willow coppice [12], which contrasts with the observations made herein. Zhao et al. then studied the pyrolysis of cigarette paper and noted that the addition of potassium inorganic and organic salts (including KCl) was likely to substantially decrease E_a (up to ~80 kJ/mol) [63]. Of note, however, Zhou et al. found no significant impact of potassium on the kinetic parameters underlying the pyrolysis of pine wood biomass impregnated with different additive contents [16]. As for Wang et al. who used the Coats–Redfern modeling approach as we did, they found that CaCl_2 was more effective than KCl in reducing the activation energy of the main pyrolysis stage of lignin, hence promoting thermal cracking reactions [28]. Consequently, and even though the results from [16,28] corroborate the conclusions drawn in the present work, further investigations considering complementary models, catalyst contents and biomass types would be quite helpful to rule on the contradictory trends sometimes emerging from the literature [12,63]. It is in fact quite difficult to compare kinetics results obtained from different works due to various factors, including the use of different biomass types, the selection of varied experimental conditions, the implementation of distinct kinetic models, etc. As a consequence, comparing the impact of various catalysts on pyrolysis kinetics would require setting exactly the same conditions both in terms of experimental and modeling approaches, as done herein. As such, the analysis proposed in this section led to consistent trends, providing interesting insights explaining the experimental observations made in Section 3.1.

3.2.2. Comparison of Measured and Simulated Conversion Degree Profiles

Although the present work did not set out to infer absolute kinetic parameters, as stressed above, we still assessed the relative validity of the E_a and A values inferred in Section 3.2.1 by comparing the simulated and measured evolutions of the conversion degree as a function of the temperature, as was done in [46,73–76]. To this end, the kinetic parameters derived in Section 3.2.1 were integrated into Equation (2), considering a D3 model, to obtain the curves plotted in Figure 5 in the case of corncob.

As can be seen, the simulated curves match well their experimental counterparts (similar results being obtained in the case of beech wood, although not reported, for brevity). Discrepancies, however, arise for $\alpha > 80\%$. This may have been expected, though, since only data free from significant measurement noise (i.e., those collected for $10\% < \alpha < 80\%$) were considered during the model-fitting process (see Section 3.2.1). It is indeed well known that model-fitting methods are mainly applicable on relatively narrow ranges of conversion degrees. Furthermore, it may be difficult to obtain a satisfactory precision in the simulation

of mass losses measured at the initial and final pyrolysis stages with such a modeling approach, as reiterated in [69].

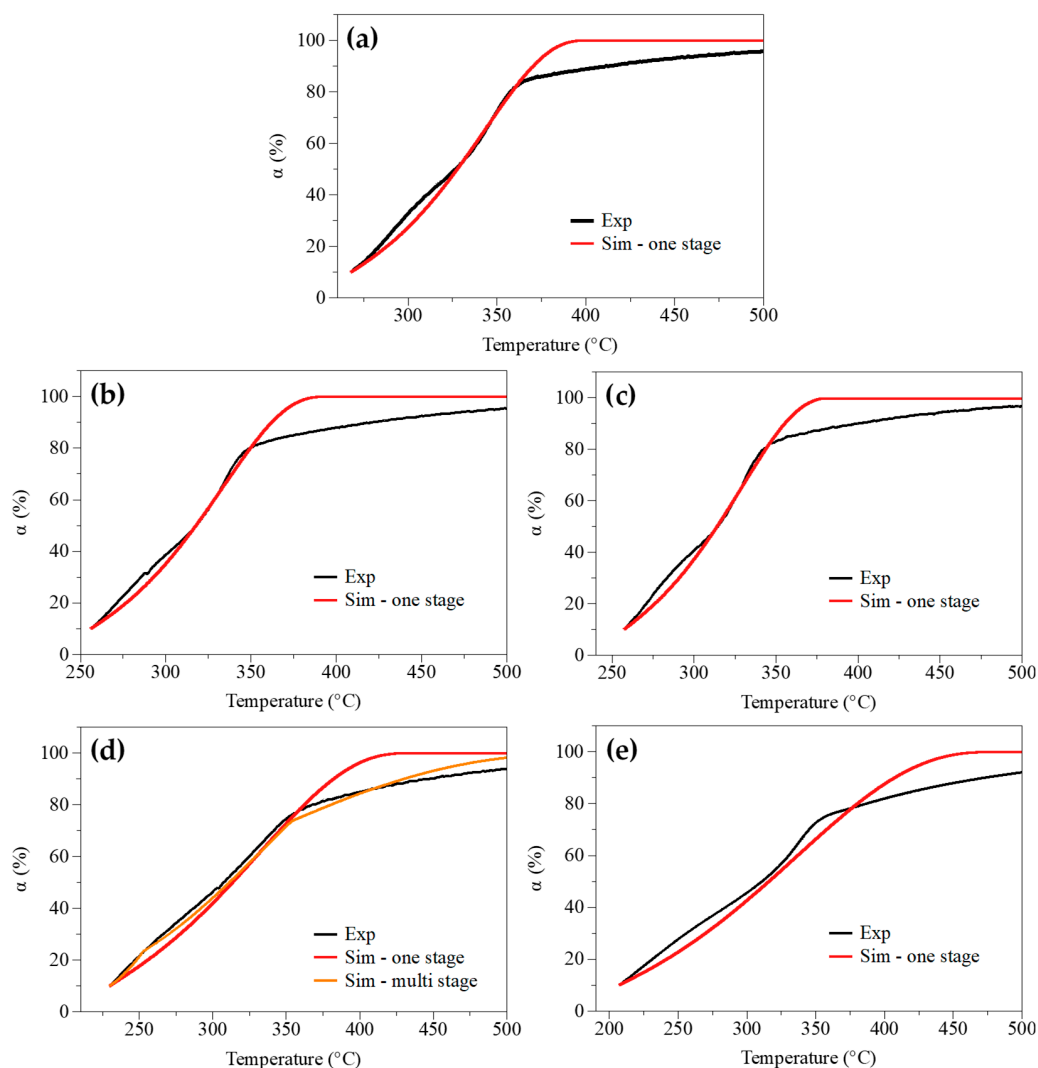


Figure 5. $\alpha = f(T)$ —Comparison of measured (Exp) and simulated (Sim) data for (a) raw corncob and samples impregnated with (b) NaCl, (c) KCl, (d) CaCl₂ and (e) MgCl₂.

This thus explains why the above α range was set. To address this issue and enable a better fitting between measured and modeled data, the whole pyrolysis process can alternatively be represented as a sequence of distinct reactions [16,28,37,46,70,77]. By applying this so-called multi-stage approach to the samples impregnated with CaCl₂ for which the lowest R^2 values were obtained, the gold curve depicted in Figure 5d is obtained. Based on a parametric study (not detailed, for brevity), we found that optimized results could be obtained by dividing the complete pyrolysis process into three stages ($\alpha < 21\%$, $21\% \leq \alpha \leq 76\%$ and $\alpha > 76\%$), for which E_a values between 32.4 and 161.9 kJ/mol were inferred (46.7 and 179.9 kJ/mol in the case of beech wood). Implementing this approach notably allows improving the agreement between experimental and simulated profiles, as shown in Figure 5d and demonstrated by R^2 values going from ~ 0.98 to ~ 0.99 . This modeling procedure will, however, not be considered further herein as it falls outside of the scope of the present work, in which kinetic analyses are only meant to facilitate the interpretation of the experimental trends highlighted with respect to the relative efficiency of the tested catalysts on the overall pyrolysis process.

3.3. Influence of the Catalyst Content

To provide a more comprehensive overview of the effects of alkaline earth metals on biomass pyrolysis as a function of the quantity of catalyst added, additional measurements were carried out with beech wood and corncob samples impregnated with CaCl_2 and MgCl_2 , considering catalyst solutions at $0.1 \times Y_0$, $0.5 \times Y_0$, and $2 \times Y_0$. The obtained results are summarized in Table 6 and Figure 6.

Table 6. Maximum mass loss rate (dTG_{\max}), characteristic temperatures determined by TGA and kinetic parameters related to the pyrolysis of beech wood, corncob and samples impregnated with CaCl_2 and MgCl_2 solutions at $0.1 \times Y_0$, $0.5 \times Y_0$, Y_0 and $2 \times Y_0$.

Sample	dTG_{\max} (wt%/min)	T_i (°C)	T_f (°C)	T_p (°C)	E_a (kJ/mol)	A (s ⁻¹)	R^2
Beech wood							
No catalyst	-4.09 [†] ; -10.37	293	380	322 [†] ; 371	150.1	1.02×10^9	0.9928
$\text{CaCl}_2-0.1 \times Y_0$	-3.45 [†] ; -6.87	279	374	304 [†] ; 352	130.9	3.14×10^7	0.9933
$\text{CaCl}_2-0.5 \times Y_0$	-3.48 [†] ; -5.45	252	369	275 [†] ; 344	101.8	1.05×10^5	0.9840
CaCl_2-Y_0	-3.67 [†] ; -3.88	252	385	258 [†] ; 355	89.4	1.17×10^4	0.9829
$\text{CaCl}_2-2 \times Y_0$	-4.06	235	385	296	81.3	3.41×10^3	0.9474
$\text{MgCl}_2-0.1 \times Y_0$	-3.19 [†] ; -8.04	271	371	294 [†] ; 353	122.9	6.46×10^6	0.9902
$\text{MgCl}_2-0.5 \times Y_0$	-2.39 [†] ; -6.97	249	369	280 [†] ; 347	94.4	2.30×10^4	0.9765
MgCl_2-Y_0	-2.40 [†] ; -6.83	233	388	234 [†] ; 355	75.2	5.09×10^2	0.9849
$\text{MgCl}_2-2 \times Y_0$	-2.45 [†] ; -2.99	208	401	248 [†] ; 315	58.5	2.35×10^1	0.9782
Corn cob							
No catalyst	-4.22 [†] ; -6.07	268	357	282 [†] ; 321	132.5	1.15×10^8	0.9788
$\text{CaCl}_2-0.1 \times Y_0$	-4.50 [†] ; -5.75	253	360	274 [†] ; 344	95.7	5.51×10^4	0.9638
$\text{CaCl}_2-0.5 \times Y_0$	-4.13 [†] ; -4.70	238	364	260 [†] ; 339	78.2	1.63×10^3	0.9596
CaCl_2-Y_0	-3.35 [†] ; -3.46	230	367	256 [†] ; 318	77.9	1.94×10^3	0.9769
$\text{CaCl}_2-2 \times Y_0$	-3.28 [†] ; -3.19	226	386	251 [†] ; 303	66.3	1.52×10^2	0.9540
$\text{MgCl}_2-0.1 \times Y_0$	-4.62 [†] ; -6.15	262	361	285 [†] ; 335	113.1	1.81×10^6	0.9727
$\text{MgCl}_2-0.5 \times Y_0$	-3.30 [†] ; -5.16	240	363	280 [†] ; 334	83.4	4.61×10^3	0.9815
MgCl_2-Y_0	-2.55 [†] ; -3.15	207	386	234 [†] ; 327	59.1	2.99×10^1	0.9831
$\text{MgCl}_2-2 \times Y_0$	-2.36 [†] ; -2.87	198	397	229 [†] ; 319	49.6	3.65×10^0	0.9876

[†] Values related to the shoulder and/or to the first dTG peak.

Overall, the higher the catalyst content, the lower the T_i and T_p values (see Table 6). Furthermore, and as previously noted in Section 3.1, MgCl_2 remains more effective than CaCl_2 in decreasing the initial pyrolysis temperature, which may be related to the ability of the former to enhance the dehydration of hemicellulose. As for the shoulder observed on the left of the main dTG peak, it tends to disappear when adding increasing quantities of catalyst (see Figure 6) in favor of the formation of two separate peaks, which may be related to the decomposition of hemicellulose and cellulose, respectively [49,50].

It may finally be noted that the higher the catalyst content, the lower the temperature of the first peak, as illustrated in Figure 6c,d,g,h. From a kinetic perspective, the data gathered in Table 6 confirm that both calcium and magnesium cations allow decreasing the activation energy of the pyrolysis reactions even at low additive contents. Furthermore, the obtained results also show that the higher the catalyst concentration, the lower the E_a values, which is in line with the reductions of T_i and T_p reported when increasing the quantities of CaCl_2 and MgCl_2 . Looking further at the activation energies inferred for the beech wood samples impregnated with CaCl_2 , it can be noted that their values go from 150.1 kJ/mol to 89.4 kJ/mol (i.e., -60.7 kJ/mol) when the metal concentration is increased from $0.1 \times Y_0$ to Y_0 , while they only decrease from 89.4 kJ/mol to 81.3 kJ/mol (i.e., -8.1 kJ/mol) when this concentration goes from Y_0 to $2 \times Y_0$. Similarly, the E_a values related to the corncob samples decrease by 54.6 kJ/mol when increasing the concentration of cations in the impregnation solution from $0.1 \times Y_0$ to Y_0 , versus 11.6 kJ/mol when increasing it from Y_0 to $2 \times Y_0$.

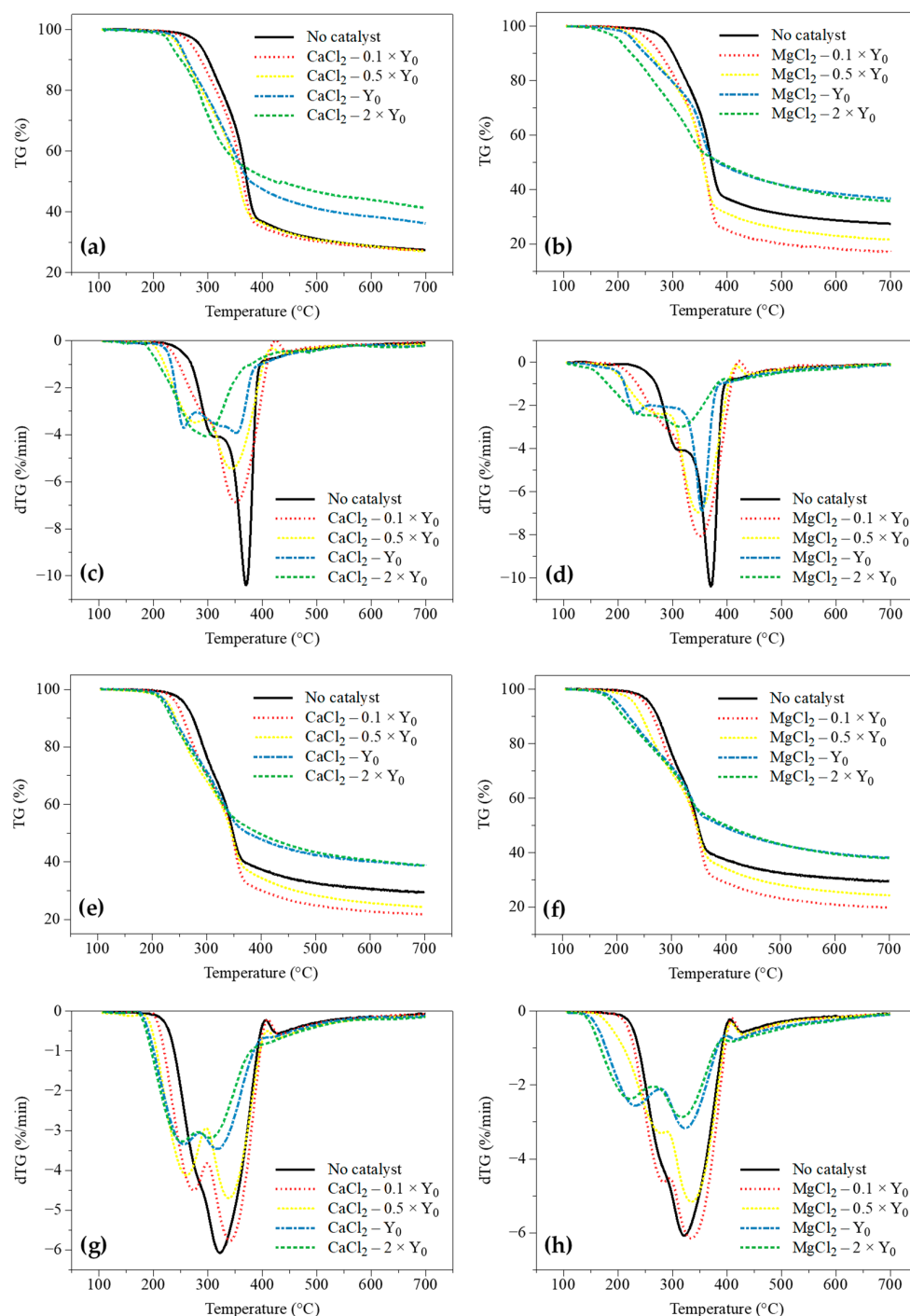


Figure 6. Evolution of the mass loss (TG) (a,b,e,f) and mass loss rate (dTG) (c,d,g,h) as a function of the temperature for beech wood (a–d) and corncob (e–h) samples impregnated with CaCl₂ and MgCl₂ solutions at $0.1 \times Y_0$, $0.5 \times Y_0$, Y_0 , and $2 \times Y_0$.

These observations thus tend to evidence the existence of a so-called saturation phenomenon (the evolution of E_a as a function of the catalyst content being asymptotic) which is also present in the case of MgCl₂ (the E_a values indeed decreasing by ~ 74 kJ/mol on average for both beech wood and corncob when the concentration of magnesium cations goes from $0.1 \times Y_0$ to Y_0 , versus ~ 13 kJ/mol when it increases from Y_0 to $2 \times Y_0$). All these observations thus tend to show that although alkaline earth metals exhibit a strong catalytic effect on biomass pyrolysis, their use at high loads does not necessarily represent an interesting option as it does not promote the process as intensively as when they are

used with low blending ratios. This is further corroborated by the fact that the higher the catalyst concentration, the lower the yield of volatile products and the higher the char yield, as shown by the TG curves of Figure 6a,b,e,f. In other words, the lower the catalyst concentration, the more optimal the use of the biomass.

4. Conclusions

This work covered an experimental analysis of the catalytic effects induced by AAEMs on the pyrolysis of biomass. In this analysis, beech wood and corncob were impregnated with various AAEM catalysts (Na_2CO_3 , NaOH , NaCl , KCl , CaCl_2 , and MgCl_2). The impact of these AAEM additives on the pyrolysis was evaluated based on maximum mass loss rates and characteristic temperatures measured by TGA, as well as on rate constant parameters derived from a model-fitting approach integrating 14 different reaction models.

In terms of highlights, the analyses conducted herein showed that AAEM catalysts can reduce the initial and peak temperatures of the pyrolysis as well as the related activation energies. More specifically, this work showed that metal cations such as Na^+ , K^+ , Ca^{2+} , and Mg^{2+} significantly influence the process. Furthermore, it was found that alkaline earth metals (i.e., calcium and magnesium) exhibit a stronger catalytic effect at low temperatures than do alkali metals, which can be traced to the strong affinity of the former to oxygenated groups present in biopolymers and to the ability of such metallic ions to induce a homolytic fission of glucose rings, the cleavage of glycosidic bonds, and dehydration reactions, together with the depolymerization of hemicellulose. The basic character of the catalysts was also demonstrated to be an important factor influencing the pyrolysis process. Basic catalysts indeed have a strong deoxygenation capability through decarboxylation, decarbonylation, and demethoxylation reactions, thus explaining why the catalytic efficiency of NaOH , Na_2CO_3 , and NaCl was found to follow their basicity order. By increasing the quantities of calcium and magnesium catalysts added to beech wood and corncob, a saturation phenomenon was finally evidenced, hence illustrating that the efficiency of alkaline earth metals in promoting the conversion of biomass is higher at relatively low contents.

This work therefore provided insights contributing to elucidate the relative impact of different AAEM catalysts added to the same feedstocks under the same conditions. Complementary works are, however, required for more thorough analysis and interpretation of the main trends reported throughout this study. Mappings of the AAEM distribution between the surface and the bulk of the biomass as well as further modeling works based on the implementation of refined global schemes or network models would notably benefit from being undertaken, thus paving the way for future works to be conducted.

Author Contributions: Conceptualization, R.L. and A.B.; methodology, W.W., R.L. and A.B.; software, W.W. and R.L.; validation, R.L.; formal analysis, W.W. and R.L.; investigation, W.W. and R.L.; resources, R.L. and A.B.; writing—original draft preparation, W.W. and R.L.; writing—review and editing, R.L.; visualization, W.W. and R.L.; supervision, R.L., A.B. and D.L.; project administration, R.L., A.B. and D.L.; funding acquisition, R.L. and A.B. All authors have read and agreed to the published version of the manuscript.

Funding: This research received support from the French Ministry of Higher Education, Research, and Innovation (Ministère de l'Enseignement supérieur, de la Recherche et de l'Innovation).

Data Availability Statement: The data presented in this study are available on request from the corresponding author.

Conflicts of Interest: The authors declare no conflict of interest.

Appendix A

The present appendix consists of a table (Table A1) which brings together the rate constant parameters derived using the 14 reaction models considered in this work for different raw and impregnated beech wood and corncob samples.

Table A1. Examples of kinetic parameters derived from the use of the F1, F2, F3, F5, F7, D1, D2, D3, R2, R3, A2, A3, A4, and P2 reaction models to simulate the TGA results obtained with beech wood, corncob, and samples impregnated with AAEM solutions at Y_0 .

Sample	F1			F2			F3			F5		
	E_a (kJ/mol)	A (s^{-1})	R^2	E_a (kJ/mol)	A (s^{-1})	R^2	E_a (kJ/mol)	A (s^{-1})	R^2	E_a (kJ/mol)	A (s^{-1})	R^2
Beech wood	76.8	6.87×10^3	0.9891	100.5	1.29×10^6	0.9698	128.5	5.75×10^8	0.9428	194.3	7.94×10^{14}	0.8966
Beech wood + NaOH	58.6	5.56×10^2	0.9710	76.7	5.01×10^4	0.9864	98.0	9.16×10^6	0.9914	148.1	1.60×10^{12}	0.9879
Beech wood + $CaCl_2$	45.0	1.42×10^1	0.9877	63.5	1.29×10^3	0.9959	85.9	2.59×10^5	0.9873	138.7	5.55×10^{10}	0.9642
Beech wood + $MgCl_2$	36.9	2.10×10^0	0.9735	51.2	7.92×10^1	0.9410	68.4	5.45×10^3	0.9066	109.0	9.04×10^7	0.8582
Corncob	67.9	2.26×10^3	0.9787	90.6	4.43×10^5	0.9861	117.6	2.14×10^8	0.9752	181.2	3.66×10^{14}	0.9469
Corncob + NaCl	63.0	1.01×10^3	0.9797	85.1	1.96×10^5	0.9806	111.6	9.46×10^7	0.9629	173.9	1.61×10^{14}	0.9276
Corncob + KCl	67.0	2.66×10^3	0.9730	90.1	6.41×10^5	0.9769	117.7	4.01×10^8	0.9626	182.7	1.26×10^{15}	0.9296
Corncob + $CaCl_2$	38.8	4.99×10^0	0.9812	55.1	3.24×10^2	0.9873	74.7	4.33×10^4	0.9844	121.2	3.51×10^9	0.9614
Corncob + $MgCl_2$	28.5	4.33×10^{-1}	0.9818	41.4	1.46×10^1	0.9827	57.1	8.78×10^2	0.9692	94.0	1.06×10^7	0.9394
Sample	F7			D1			D2			D3		
	E_a (kJ/mol)	A (s^{-1})	R^2	E_a (kJ/mol)	A (s^{-1})	R^2	E_a (kJ/mol)	A (s^{-1})	R^2	E_a (kJ/mol)	A (s^{-1})	R^2
Beech wood	268.2	5.35×10^{21}	0.8697	125.8	4.54×10^7	0.9908	137.0	2.65×10^8	0.9930	150.1	1.02×10^9	0.9928
Beech wood + NaOH	204.7	1.15×10^{18}	0.9814	97.0	9.88×10^5	0.9509	105.7	4.23×10^6	0.9600	115.8	1.11×10^7	0.9687
Beech wood + $CaCl_2$	197.6	4.04×10^{16}	0.9502	71.2	1.39×10^3	0.9575	79.5	5.06×10^3	0.9711	89.4	1.19×10^4	0.9829
Beech wood + $MgCl_2$	154.2	3.84×10^{12}	0.8342	60.9	1.35×10^2	0.9896	67.4	3.41×10^2	0.9890	75.2	5.09×10^2	0.9849
Corncob	252.5	3.06×10^{21}	0.9285	109.5	5.22×10^6	0.9591	120.1	2.99×10^7	0.9698	132.5	1.15×10^8	0.9788
Corncob + NaCl	243.6	1.28×10^{21}	0.9071	100.9	1.23×10^6	0.9682	111.0	6.74×10^6	0.9772	123.0	2.50×10^7	0.9840
Corncob + KCl	255.6	2.03×10^{22}	0.9098	107.1	5.38×10^6	0.9594	117.7	3.31×10^7	0.9694	130.3	1.40×10^8	0.9773
Corncob + $CaCl_2$	172.9	8.70×10^{14}	0.9474	61.9	3.12×10^2	0.9482	69.2	9.83×10^2	0.9636	77.9	1.94×10^3	0.9769
Corncob + $MgCl_2$	135.2	3.03×10^{11}	0.9233	46.5	9.47×10^0	0.9596	52.2	2.19×10^1	0.9729	59.1	2.99×10^1	0.9831

Table A1. Cont.

Sample	R2			R3			A2			A3		
	E _a (kJ/mol)	A (s ⁻¹)	R ²	E _a (kJ/mol)	A (s ⁻¹)	R ²	E _a (kJ/mol)	A (s ⁻¹)	R ²	E _a (kJ/mol)	A (s ⁻¹)	R ²
Beech wood	66.8	3.58 × 10 ²	0.9921	70.0	4.94 × 10 ²	0.9917	33.4	8.54 × 10 ⁻¹	0.9858	18.9	3.18 × 10 ⁻²	0.9806
Beech wood + NaOH	50.8	3.88 × 10 ¹	0.9576	53.3	4.89 × 10 ¹	0.9625	24.7	2.25 × 10 ⁻¹	0.9581	13.4	1.20 × 10 ⁻²	0.9357
Beech wood + CaCl ₂	37.4	1.04 × 10 ⁰	0.9708	39.8	1.28 × 10 ⁰	0.9776	17.6	2.77 × 10 ⁻²	0.9781	8.5	2.28 × 10 ⁻³	0.9553
Beech wood + MgCl ₂	30.9	2.20 × 10 ⁻¹	0.9834	32.8	2.42 × 10 ⁻¹	0.9809	13.6	9.24 × 10 ⁻³	0.9554	5.9	9.10 × 10 ⁻⁴	0.9053
Corncob	58.3	1.17 × 10 ²	0.9703	61.4	1.61 × 10 ²	0.9751	29.1	4.73 × 10 ⁻¹	0.9751	16.2	2.07 × 10 ⁻²	0.9636
Corncob + NaCl	53.8	5.34 × 10 ¹	0.9775	56.7	7.33 × 10 ¹	0.9810	26.8	3.08 × 10 ⁻¹	0.9792	14.7	1.51 × 10 ⁻²	0.9689
Corncob + KCl	57.3	1.27 × 10 ²	0.9693	60.4	1.80 × 10 ²	0.9735	28.8	5.22 × 10 ⁻¹	0.9712	16.0	2.24 × 10 ⁻²	0.9586
Corncob + CaCl ₂	32.1	4.18 × 10 ⁻¹	0.9611	34.2	4.95 × 10 ⁻¹	0.9692	14.7	1.53 × 10 ⁻²	0.9650	6.7	1.39 × 10 ⁻³	0.9215
Corncob + MgCl ₂	23.2	4.75 × 10 ⁻²	0.9677	24.9	5.16 × 10 ⁻²	0.9748	9.6	3.44 × 10 ⁻³	0.9610	3.3	3.37 × 10 ⁻⁴	0.8517
Sample	A4			P2								
	E _a (kJ/mol)	A (s ⁻¹)	R ²	E _a (kJ/mol)	A (s ⁻¹)	R ²						
Beech wood	11.6	5.04 × 10 ⁻³	0.9720	23.9	8.24 × 10 ⁻²	0.9831						
Beech wood + NaOH	7.7	2.18 × 10 ⁻³	0.8925	17.3	2.80 × 10 ⁻²	0.9033						
Beech wood + CaCl ₂	3.9	4.34 × 10 ⁻⁴	0.8814	10.5	3.25 × 10 ⁻³	0.8751						
Beech wood + MgCl ₂	2.0	1.48 × 10 ⁻⁴	0.6774	8.0	1.48 × 10 ⁻³	0.9605						
Corncob	9.7	3.48 × 10 ⁻³	0.9428	20.1	4.44 × 10 ⁻²	0.9235						
Corncob + NaCl	8.6	2.65 × 10 ⁻³	0.9493	18.1	2.91 × 10 ⁻²	0.9368						
Corncob + KCl	9.6	3.74 × 10 ⁻³	0.9362	19.6	4.55 × 10 ⁻²	0.9243						
Corncob + CaCl ₂	2.6	2.46 × 10 ⁻⁴	0.7512	8.4	1.96 × 10 ⁻³	0.8289						
Corncob + MgCl ₂	0.1	6.07 × 10 ⁻⁶	0.0102	4.6	4.87 × 10 ⁻⁴	0.7526						

References

1. Deng, S.; Wang, X.; Zhang, J.; Liu, Z.; Mikulčić, H.; Vujanović, M.; Tan, H.; Duić, N. A kinetic study on the catalysis of KCl, K₂SO₄, and K₂CO₃ during oxy-biomass combustion. *J. Environ. Manag.* **2018**, *218*, 50–58. [[CrossRef](#)] [[PubMed](#)]
2. Collard, F.-X.; Blin, J. A review on pyrolysis of biomass constituents: Mechanisms and composition of the products obtained from the conversion of cellulose, hemicelluloses and lignin. *Renew. Sustain. Energy Rev.* **2014**, *38*, 594–608. [[CrossRef](#)]
3. Norouzi, O.; Taghavi, S.; Arku, P.; Jafarian, S.; Signoretto, M.; Dutta, A. What is the best catalyst for biomass pyrolysis? *J. Anal. Appl. Pyrolysis* **2021**, *158*, 105280. [[CrossRef](#)]
4. Qiu, B.; Tao, X.; Wang, J.; Liu, Y.; Li, S.; Chu, H. Research progress in the preparation of high-quality liquid fuels and chemicals by catalytic pyrolysis of biomass: A review. *Energy Convers. Manag.* **2022**, *261*, 115647. [[CrossRef](#)]
5. Kabir, G.; Hameed, B.H. Recent progress on catalytic pyrolysis of lignocellulosic biomass to high-grade bio-oil and bio-chemicals. *Renew. Sustain. Energy Rev.* **2017**, *70*, 945–967. [[CrossRef](#)]
6. Chen, X.; Che, Q.; Li, S.; Liu, Z.; Yang, H.; Chen, Y.; Wang, X.; Shao, J.; Chen, H. Recent developments in lignocellulosic biomass catalytic fast pyrolysis: Strategies for the optimization of bio-oil quality and yield. *Fuel Process. Technol.* **2019**, *196*, 106180. [[CrossRef](#)]
7. Wang, W.; Lemaire, R.; Bensakhria, A.; Luart, D. Review on the catalytic effects of alkali and alkaline earth metals (AAEMs) including sodium, potassium, calcium and magnesium on the pyrolysis of lignocellulosic biomass and on the co-pyrolysis of coal with biomass. *J. Anal. Appl. Pyrolysis* **2022**, *163*, 105479. [[CrossRef](#)]
8. Shimada, N.; Kawamoto, H.; Saka, S. Different action of alkali/alkaline earth metal chlorides on cellulose pyrolysis. *J. Anal. Appl. Pyrolysis* **2008**, *81*, 80–87. [[CrossRef](#)]
9. Siriwardane, R.V.; Poston, J.A.; Robinson, C.; Simonyi, T. Effect of additives on decomposition of sodium carbonate: Precombustion CO₂ capture sorbent regeneration. *Energy Fuels* **2011**, *25*, 1284–1293. [[CrossRef](#)]
10. Hwang, H.; Oh, S.; Choi, I.-G.; Choi, J.W. Catalytic effects of magnesium on the characteristics of fast pyrolysis products—Bio-oil, bio-char, and non-condensed pyrolytic gas fractions. *J. Anal. Appl. Pyrolysis* **2015**, *113*, 27–34. [[CrossRef](#)]
11. Eschenbacher, A.; Fennell, P.; Jensen, A.D. A review of recent research on catalytic biomass pyrolysis and low-pressure hydro-pyrolysis. *Energy Fuels* **2021**, *35*, 18333–18369. [[CrossRef](#)]
12. Nowakowski, D.J.; Jones, J.M.; Brydson, R.M.D.; Ross, A.B. Potassium catalysis in the pyrolysis behaviour of short rotation willow coppice. *Fuel* **2007**, *86*, 2389–2402. [[CrossRef](#)]
13. Han, L.; Wang, Q.; Ma, Q.; Yu, C.; Luo, Z.; Cen, K. Influence of CaO additives on wheat-straw pyrolysis as determined by TG-FTIR analysis. *J. Anal. Appl. Pyrolysis* **2010**, *88*, 199–206. [[CrossRef](#)]
14. Wu, H.; Zhao, Z.; Zhang, W.; Li, H.; He, F. Effects of alkali/alkaline earth metals on pyrolysis characteristics of cellulose. *Trans. CSAE* **2012**, *28*, 215–220.
15. Wu, H.; Li, H.; Zhao, Z. The effect of potassium on pyrolysis characteristics of cellulose. *Acta Energ. Sol. Sin.* **2010**, *31*, 1537–1542.
16. Zhou, L.; Jia, Y.; Nguyen, T.-H.; Adesina, A.A.; Liu, Z. Hydro-pyrolysis characteristics and kinetics of potassium-impregnated pine wood. *Fuel Process. Technol.* **2013**, *116*, 149–157. [[CrossRef](#)]
17. Wang, W.; Lemaire, R.; Bensakhria, A.; Luart, D. Thermogravimetric analysis and kinetic modeling of the co-pyrolysis of a bituminous coal and poplar wood. *Chin. J. Chem. Eng.* **2022**, *in press*. [[CrossRef](#)]
18. Wang, W.; Lemaire, R.; Bensakhria, A.; Luart, D. Thermogravimetric analysis and kinetic modeling of the AAEM-catalyzed pyrolysis of woody biomass. *Molecules* **2022**, *27*, 7662. [[CrossRef](#)]
19. Trubetskaya, A.; Larsen, F.H.; Shchukarev, A.; Ståhl, K.; Umeki, K. Potassium and soot interaction in fast biomass pyrolysis at high temperatures. *Fuel* **2018**, *225*, 89–94. [[CrossRef](#)]
20. Wang, M.; Tian, J.; Roberts, D.G.; Chang, L.; Xie, K. Interactions between corncob and lignite during temperature-programmed co-pyrolysis. *Fuel* **2015**, *142*, 102–108. [[CrossRef](#)]
21. Rabemanolontsoa, H.; Saka, S. Comparative study on chemical composition of various biomass species. *RSC Adv.* **2013**, *3*, 3946–3956. [[CrossRef](#)]
22. Ding, Y.; Ezekoye, O.A.; Lu, S.; Wang, C. Thermal degradation of beech wood with thermogravimetry/Fourier transform infrared analysis. *Energy Convers. Manag.* **2016**, *120*, 370–377. [[CrossRef](#)]
23. Pointner, M.; Kuttner, P.; Obrlik, T.; Jäger, A.; Kahr, H. Composition of corncob as a substrate for fermentation of biofuels. *Agron. Res.* **2014**, *12*, 391–396.
24. Singh, H.K.; Patil, T.; Vineeth, S.; Das, S.K.; Pramanik, A.; Mhaske, S.T. Isolation of microcrystalline cellulose from corn stover with emphasis on its constituents: Corn cover and corn cob. *Mater. Today Proc.* **2020**, *27*, 589–594. [[CrossRef](#)]
25. Wang, J.; Zhang, M.; Chen, M.; Min, F.; Zhang, S.; Ren, Z.; Yan, Y. Catalytic effects of six inorganic compounds on pyrolysis of three kinds of biomass. *Thermochim. Acta* **2006**, *444*, 110–114. [[CrossRef](#)]
26. Chen, M.; Wang, J.; Zhang, M.; Chen, M.; Zhu, X.; Min, F.; Tan, Z. Catalytic effects of eight inorganic additives on pyrolysis of pine wood sawdust by microwave heating. *J. Anal. Appl. Pyrolysis* **2008**, *82*, 145–150. [[CrossRef](#)]
27. Yu, Y.; Liu, D.; Wu, H. Formation and characteristics of reaction intermediates from the fast pyrolysis of NaCl- and MgCl₂-loaded celluloses. *Energy Fuels* **2014**, *28*, 245–253. [[CrossRef](#)]
28. Wang, W.-L.; Ren, X.-Y.; Li, L.-F.; Chang, J.-M.; Cai, L.-P.; Geng, J. Catalytic effect of metal chlorides on analytical pyrolysis of alkali lignin. *Fuel Process. Technol.* **2015**, *134*, 345–351. [[CrossRef](#)]

29. Zhou, W.; Bai, B.; Chen, G.; Ma, L.; Jing, D.; Yan, B. Study on catalytic properties of potassium carbonate during the process of sawdust pyrolysis. *Int. J. Hydrogen Energy* **2018**, *43*, 13829–13841. [[CrossRef](#)]
30. Safar, M.; Lin, B.-J.; Chen, W.-H.; Langauer, D.; Chang, J.-S.; Raclavska, H.; Pétrissans, A.; Rousset, P.; Pétrissans, M. Catalytic effects of potassium on biomass pyrolysis, combustion and torrefaction. *Appl. Energy* **2019**, *235*, 346–355. [[CrossRef](#)]
31. Haddad, K.; Jeguirim, M.; Jellali, S.; Guizani, C.; Delmotte, L.; Bennici, S.; Limousy, L. Combined NMR structural characterization and thermogravimetric analyses for the assessment of the AAEM effect during lignocellulosic biomass pyrolysis. *Energy* **2017**, *134*, 10–23. [[CrossRef](#)]
32. dos Santos, J.C.; Siqueira, R.L.; Vieira, L.M.G.; Freire, R.T.S.; Mano, V.; Panzera, T.H. Effects of sodium carbonate on the performance of epoxy and polyester coir-reinforced composites. *Polym. Test.* **2018**, *67*, 533–544. [[CrossRef](#)]
33. Guo, F.; Liu, Y.; Wang, Y.; Li, X.; Li, T.; Guo, C. Pyrolysis kinetics and behavior of potassium-impregnated pine wood in TGA and a fixed-bed reactor. *Energy Convers. Manag.* **2016**, *130*, 184–191. [[CrossRef](#)]
34. Qin, Q.; Zhou, J.; Lin, B.; Xie, C.; Zhou, L. Influence of coal ash on the characteristics of corn straw pyrolysis products. *Bioresour. Technol.* **2020**, *318*, 124055. [[CrossRef](#)] [[PubMed](#)]
35. Vyazovkin, S.; Burnham, A.K.; Criado, J.M.; Pérez-Maqueda, L.A.; Popescu, C.; Sbirrazzuoli, N. ICTAC Kinetics Committee recommendations for performing kinetic computations on thermal analysis data. *Thermochim. Acta* **2011**, *520*, 1–19. [[CrossRef](#)]
36. Vyazovkin, S.; Chrissafis, K.; Di Lorenzo, M.L.; Koga, N.; Pijolat, M.; Roduit, B.; Sbirrazzuoli, N.; Suñol, J.J. ICTAC Kinetics Committee recommendations for collecting experimental thermal analysis data for kinetic computations. *Thermochim. Acta* **2014**, *590*, 1–23. [[CrossRef](#)]
37. Ye, J.; Jin, C.; Song, P.; Wu, Q. Pyrolysis kinetics of alkali lignin catalyzed by sodium carbonate. *Chem. Ind. For. Prod.* **2010**, *30*, 40–44.
38. Varma, A.K.; Mondal, P. Physicochemical characterization and kinetic study of pine needle for pyrolysis process. *J. Therm. Anal. Calorim.* **2016**, *124*, 487–497. [[CrossRef](#)]
39. Loy, A.C.M.; Yusup, S.; Chin, B.L.F.; Gan, D.K.W.; Shahbaz, M.; Acda, M.N.; Unrean, P.; Rianawati, E. Comparative study of in-situ catalytic pyrolysis of rice husk for syngas production: Kinetics modelling and product gas analysis. *J. Clean. Prod.* **2018**, *197*, 1231–1243. [[CrossRef](#)]
40. Mian, I.; Li, X.; Jian, Y.; Dacres, O.D.; Zhong, M.; Liu, J.; Ma, F.; Rahman, N. Kinetic study of biomass pellet pyrolysis by using distributed activation energy model and Coats Redfern methods and their comparison. *Bioresour. Technol.* **2019**, *294*, 122099. [[CrossRef](#)]
41. Gupta, A.; Thengane, S.K.; Mahajani, S. Kinetics of pyrolysis and gasification of cotton stalk in the central parts of India. *Fuel* **2020**, *263*, 116752. [[CrossRef](#)]
42. Sattar, H.; Muzaffar, I.; Munir, S. Thermal and kinetic study of rice husk, corn cobs, peanut crust and Khushab coal under inert (N₂) and oxidative (dry air) atmospheres. *Renew. Energy* **2020**, *149*, 794–805. [[CrossRef](#)]
43. Xiao, R.; Yang, W.; Cong, X.; Dong, K.; Xu, J.; Wang, D.; Yang, X. Thermogravimetric analysis and reaction kinetics of lignocellulosic biomass pyrolysis. *Energy* **2020**, *201*, 117537. [[CrossRef](#)]
44. Zhu, L.; Zhong, Z. Effects of cellulose, hemicellulose and lignin on biomass pyrolysis kinetics. *Korean J. Chem. Eng.* **2020**, *37*, 1660–1668. [[CrossRef](#)]
45. Sahoo, A.; Kumar, S.; Kumar, J.; Bhaskar, T. A detailed assessment of pyrolysis kinetics of invasive lignocellulosic biomasses (*Prosopis juliflora* and *Lantana camara*) by thermogravimetric analysis. *Bioresour. Technol.* **2021**, *319*, 124060. [[CrossRef](#)] [[PubMed](#)]
46. Li, J.; Dou, B.; Zhang, H.; Zhang, H.; Chen, H.; Xu, Y. Thermochemical characteristics and non-isothermal kinetics of camphor biomass waste. *J. Environ. Chem. Eng.* **2021**, *9*, 105311. [[CrossRef](#)]
47. Wang, W.; Lemaire, R. Global kinetic modeling of the devolatilization of pulverized coal and poplar wood in a thermogravimetric analyzer and a flat flame reactor. In Proceedings of the Combustion Institute—Canadian Section, Spring Technical Meeting, Ottawa, ON, Canada, 16–19 May 2022.
48. Coats, A.W.; Redfern, J.P. Kinetic parameters from thermogravimetric data. *Nature* **1964**, *201*, 68–69. [[CrossRef](#)]
49. Helsen, L.; Van den Bulck, E. Kinetics of the low-temperature pyrolysis of chromated copper arsenate-treated wood. *J. Anal. Appl. Pyrolysis* **2000**, *53*, 51–79. [[CrossRef](#)]
50. Chen, Z.; Hu, M.; Zhu, X.; Guo, D.; Liu, S.; Hu, Z.; Xiao, B.; Wang, J.; Laghari, M. Characteristics and kinetic study on pyrolysis of five lignocellulosic biomass via thermogravimetric analysis. *Bioresour. Technol.* **2015**, *192*, 441–450. [[CrossRef](#)]
51. Zhao, N.; Li, B.-X. The effect of sodium chloride on the pyrolysis of rice husk. *Appl. Energy* **2016**, *178*, 346–352. [[CrossRef](#)]
52. Peng, C.; Zhang, G.; Yue, J.; Xu, G. Pyrolysis of lignin for phenols with alkaline additive. *Fuel Process. Technol.* **2014**, *124*, 212–221. [[CrossRef](#)]
53. Rutkowski, P. Pyrolysis of cellulose, xylan and lignin with the K₂CO₃ and ZnCl₂ addition for bio-oil production. *Fuel Process. Technol.* **2011**, *92*, 517–522. [[CrossRef](#)]
54. Wang, Z.; Wang, F.; Cao, J.; Wang, J. Pyrolysis of pine wood in a slowly heating fixed-bed reactor: Potassium carbonate versus calcium hydroxide as a catalyst. *Fuel Process. Technol.* **2010**, *91*, 942–950. [[CrossRef](#)]
55. Katanaki, E.; Vamvuka, D.; Grammelis, P.; Kakaras, E. Thermogravimetric studies of the behavior of lignite–biomass blends during devolatilization. *Fuel Process. Technol.* **2002**, *77–78*, 159–166. [[CrossRef](#)]
56. Yang, H.; Yan, R.; Chen, H.; Lee, D.H.; Zheng, C. Characteristics of hemicellulose, cellulose and lignin pyrolysis. *Fuel* **2007**, *86*, 1781–1788. [[CrossRef](#)]

57. Mohammed, I.Y.; Abakr, Y.A.; Kazi, F.K.; Yusup, S.; Alshareef, I.; Chin, S.A. Comprehensive characterization of napier grass as a feedstock for thermochemical conversion. *Energies* **2015**, *8*, 3403–3417. [[CrossRef](#)]
58. Modenbach, A.A.; Nokes, S.E. Effects of Sodium Hydroxide Pretreatment on Structural Components of Biomass. *Trans. ASABE* **2014**, *57*, 1187–1198. [[CrossRef](#)]
59. Madorsky, S.L.; Hart, V.E.; Straus, S. Pyrolysis of cellulose in a vacuum. *J. Res. Natl. Inst. Stand. Technol.* **1956**, *56*, 343–354. [[CrossRef](#)]
60. Patwardhan, P.R.; Satrio, J.A.; Brown, R.C.; Shanks, B.H. Influence of inorganic salts on the primary pyrolysis products of cellulose. *Bioresour. Technol.* **2010**, *101*, 4646–4655. [[CrossRef](#)]
61. Kawamoto, H.; Yamamoto, D.; Saka, S. Influence of neutral inorganic chlorides on primary and secondary char formation from cellulose. *J. Wood Sci.* **2008**, *54*, 242–246. [[CrossRef](#)]
62. Eom, I.-Y.; Kim, J.-Y.; Kim, T.-S.; Lee, S.-M.; Choi, D.; Choi, I.-G.; Choi, J.-W. Effect of essential inorganic metals on primary thermal degradation of lignocellulosic biomass. *Bioresour. Technol.* **2012**, *104*, 687–694. [[CrossRef](#)] [[PubMed](#)]
63. Zhao, D.; Dai, Y.; Chen, K.; Sun, Y.; Yang, F.; Chen, K. Effect of potassium inorganic and organic salts on the pyrolysis kinetics of cigarette paper. *J. Anal. Appl. Pyrolysis* **2013**, *102*, 114–123. [[CrossRef](#)]
64. Zhu, C.; Maduskar, S.; Paulsen, A.D.; Dauenhauer, P.J. Alkaline-earth-metal-catalyzed thin-film pyrolysis of cellulose. *Chem-CatChem* **2016**, *8*, 818–829. [[CrossRef](#)]
65. Leng, E.; Wang, Y.; Gong, X.; Zhang, B.; Zhang, Y.; Xu, M. Effect of KCl and CaCl₂ loading on the formation of reaction intermediates during cellulose fast pyrolysis. *Proc. Combust. Inst.* **2017**, *36*, 2263–2270. [[CrossRef](#)]
66. Santana, J.A.; Sousa, N.G.; Cardoso, C.R.; Carvalho, W.S.; Ataíde, C.H. Sodium, zinc and magnesium chlorides as additives for soybean hulls pyrolysis: Influence on the temperature range of reactions and product selectivity. *J. Therm. Anal. Calorim.* **2016**, *125*, 471–481. [[CrossRef](#)]
67. Liu, D.; Yu, Y.; Long, Y.; Wu, H. Effect of MgCl₂ loading on the evolution of reaction intermediates during cellulose fast pyrolysis at 325 °C. *Proc. Combust. Inst.* **2015**, *35*, 2381–2388. [[CrossRef](#)]
68. Yang, C.; Yao, J.; Lin, W.; Ding, Y.; Liu, S. Influence of minerals on biomass pyrolysis and its solution. *Chem. Bioeng.* **2005**, *10*, 17–19.
69. Wang, S.; Dai, G.; Yang, H.; Luo, Z. Lignocellulosic biomass pyrolysis mechanism: A state-of-the-art review. *Prog. Energy Combust. Sci.* **2017**, *62*, 33–86. [[CrossRef](#)]
70. Naqvi, S.R.; Uemura, Y.; Osman, N.; Yusup, S. Kinetic study of the catalytic pyrolysis of paddy husk by use of thermogravimetric data and the Coats–Redfern model. *Res. Chem. Intermed.* **2015**, *41*, 9743–9755. [[CrossRef](#)]
71. Balasundram, V.; Ibrahim, N.; Kasmani, R.M.; Hamid, M.K.A.; Isha, R.; Hasbullah, H.; Ali, R.R. Thermogravimetric catalytic pyrolysis and kinetic studies of coconut copra and rice husk for possible maximum production of pyrolysis oil. *J. Clean. Prod.* **2017**, *167*, 218–228. [[CrossRef](#)]
72. Shimada, N.; Kawamoto, H.; Saka, S. Solid-state hydrolysis of cellulose and methyl α - and β -d-glucopyranosides in presence of magnesium chloride. *Carbohydr. Res.* **2007**, *342*, 1373–1377. [[CrossRef](#)] [[PubMed](#)]
73. Xu, Y.; Zhang, Y.; Zhang, G.; Guo, Y.; Zhang, J.; Li, G. Pyrolysis characteristics and kinetics of two Chinese low-rank coals. *J. Therm. Anal. Calorim.* **2015**, *122*, 975–984. [[CrossRef](#)]
74. Xing, L.; Qu, Y.; Wang, C.; Shao, L.; Zou, Z.; Song, W. Kinetic study on thermal decomposition behavior of hematite ore fines at high temperature. *Metall. Mater. Trans. B* **2020**, *51*, 395–406. [[CrossRef](#)]
75. Zhang, H.; Dou, B.; Zhang, H.; Li, J.; Ruan, C.; Wu, C. Study on non-isothermal kinetics and the influence of calcium oxide on hydrogen production during bituminous coal pyrolysis. *J. Anal. Appl. Pyrolysis* **2020**, *150*, 104888. [[CrossRef](#)]
76. Zhang, J.; Ding, Y.; Du, W.; Lu, K.; Sun, L. Study on pyrolysis kinetics and reaction mechanism of Beizao oil shale. *Fuel* **2021**, *296*, 120696. [[CrossRef](#)]
77. Wu, H.; Li, H.; Zhao, Z. Thermogravimetric analysis and pyrolytic kinetic study on coal/biomass blends. *J. Fuel Chem. Technol.* **2009**, *37*, 538–545.